4904 *Chem. Mater.* **2010,** *22,* 4904–4911
DOI:10.1021/cm100916m

CHEMISTRY OF MATERIALS
Article

Carbon Nanotubes with Catalyst Controlled Chiral Angle

Krzysztof K. K. Koziol,* Cate Ducati, and Alan H. Windle

Department of Materials Science, University of Cambridge, Pembroke Street, Cambridge CB2 3QZ, United Kingdom

Received March 31, 2010. Revised Manuscript Received June 24, 2010

The control of the structure of carbon nanotubes remains a central issue in rapidly developing science and technology. Of the various structural parameters of nanotubes, namely, diameters, number of walls, length, and chirality, it is the control of chirality which presents significant challenges as well as opportunities. It is known from our earlier work that the addition of nitrogen as a heterocyclic compound in the hydrocarbon feedstock leads to the growth of carpets of multiwall nanotubes in which all the walls are either of the armchair or zigzag structure. The research here shows the role of nitrogen in stabilizing iron carbide catalyst particles, the belt nucleation of the nanotubes, the orientational relationship between particle and nanotube structure, and the reconstruction of the surface layers of the carbide in contact with the growing ends of the tubes. By combining the various pieces of new experimental evidence it has proved possible to suggest why such unique types of nanotubes should form and thus lay the basis for future strategies for the synthesis of different types of nanotube with controlled chirality.

Introduction

Axial electrical properties, in particular, are highly dependent on chirality, and range from metallic to semiconducting as a function of chiral angle. While strategies for sorting of nanotubes by chirality look promising,[1] the ultimate objective must be to make exactly the right type of nanotube at the synthesis stage. There have been a number of attempts to correlate carbon nanotube synthesis parameters, such as the structure and/or composition of the catalyst particles employed in the CNT synthesis, with the chiral angles.[2−21] However, the synthesis of nanotubes with controlled chiral angles across the whole batch remains a big challenge in the field.

This paper builds on a previously reported observation from our laboratory[22] of multiwall carbon nanotubes in which all the layers have the same chiral angle, with the majority of the tubes having either of the two degenerate chiralities, that is, with the so-called zigzag or armchair structures with chiral angles of 0° and 30°, respectively. A subsequent paper explored the structural aspects of the nanotubes in more detail;[23] however, there was at that time no clear explanation of the observations and thus no emergent strategy which could be more widely applicable, for example, to single wall carbon nanotubes or graphene layers. The work we report here provides such an understanding which forms a base for subsequent, much more wide ranging, studies. The paper shows first that the role of a nitrogen containing component of the hydrocarbon "feedstock" is the stabilization of iron carbide rather than iron as the catalyst material. It then discusses the unique growth mechanism of the multiwall nanotubes with a catalyst particle at each end

*To whom correspondence should be addressed. E-mail: kk292@cam.ac.uk.

(1) Arnold, M. S.; Green, A. A.; Hulvat, J. F.; Stupp, S. I.; Hersam, M. C. *Nat. Nanotechnol.* **2006**, *1*, 60.
(2) Bachilo, S. M.; Balzano, L.; Herrera, J. E.; Pompeo, F.; Resasco, D. E.; Weisman, R. B. *J. Am. Chem. Soc.* **2003**, *125*, 11186.
(3) Miyauchi, Y.; Chiashi, S.; Murakami, Y.; Hayashida, Y.; Maruyama, S. *Chem. Phys. Lett.* **2004**, *387*, 198.
(4) Li, X. L.; Tu, X.; Zaric, S.; Welsher, K.; Seo, W. S.; Zhao, W.; Dai, H. *J. Am. Chem. Soc.* **2007**, *129*, 15770.
(5) Duesberg, G. S.; Graham, A. P.; Liebau, M.; Seidel, R.; Unger, E.; Kreupl, F.; Hoenlein, W. *Nano Lett.* **2003**, *3*, 257.
(6) Li, Y.; Peng, S.; Mann, D.; Cao, J.; Tu, R.; Cho, K. J.; Dai, H. *J. Phys. Chem. B* **2005**, *109*, 6968.
(7) Zhang, G. Y.; Qi, P.; Wang, X.; Lu, Y.; Li, X.; Tu, R.; Bangsaruntip, S.; Mann, D.; Zhang, L.; Dai, H. *Science* **2006**, *314*, 974.
(8) Ago, H.; Imamura, S.; Okazaki, T.; Saito, T.; Yumura, M.; Tsuji, M. *J. Phys. Chem. B* **2005**, *109*, 10035.
(9) Lolli, G.; Zhang, L.; Balzano, L.; Sakulchaicharoen, N.; Tan, Y.; Resasco, D. E. *J. Phys. Chem. B* **2006**, *110*, 2108.
(10) Wang, B.; Wei, L.; Yao, L.; Li, L.-J.; Yang, Y.; Chen, Y. *J. Phys. Chem. C* **2007**, *111*, 14612.
(11) Wang, B.; Poa, C. H. P.; Wei, L.; Li, L.-J.; Yang, Y.; Chen, Y. *J. Am. Chem. Soc.* **2007**, *129*, 9014.
(12) Li, Y. M.; Kim, W.; Zhang, Y.; Rolandi, M.; Wang, D.; Dai, H. *J. Phys. Chem. B* **2001**, *105*, 11424.
(13) Bandow, S.; Asaka, S.; Saito, Y.; Rao, A. M.; Grigorian, L.; Eklund, P. C. *Phys. Rev. Lett.* **1998**, *80*, 3779.
(14) Hongo, H.; Yudasaka, M.; Ichihashi, T.; Nihey, F.; Iijima, S. *Chem. Phys. Lett.* **2002**, *361*, 349.
(15) Kusunoki, M.; Suzuki, T.; Honjo, C.; Hirayama, T.; Shibata, N. *Chem. Phys. Lett.* **2002**, *366*, 458.
(16) Hayashi, K.; Mizuno, S.; Tanaka, S.; Toyoda, H.; Tochihara, H.; Suemune, I. *Jpn. J. Appl. Phys.* **2005**, *44*, L803–L805.
(17) Kunstmann, J.; Quandt, A.; Boustani, I. *Nanotechnology* **2007**, *18*, 155703.
(18) Ishigami, N.; Ago, H.; Imamoto, K.; Tsuji, M.; Iakoubovskii, K.; Minami, N. *J. Am. Chem. Soc.* **2008**, *130*, 9918.
(19) Gargate, R. V.; Banerjee, D. *Scanning* **2008**, *30*, 151.
(20) Harutyunyan, A. R.; Chen, G.; Paronyan, T. M.; Pigos, E. M.; Kuznetsov, O. A.; Hewaparakrama, K.; Kim, S. M.; Zakharov, D.; Stach, E. A.; Sumanasekera, G. U. *Science* **2009**, *326*, 116.
(21) Chiang, W.-H.; Sankaran, R. M. *Nat. Mater.* **2009**, *8*, 882.
(22) Koziol, K.; Shaffer, M.; Windle, A. *Adv. Mater.* **2005**, *17*, 760.
(23) Ducati, C.; Koziol, K.; Friedrichs, S.; Yates, T. J. V.; Shaffer, M. S.; Midgley, P. A.; Windle, A. H. *Small* **2006**, *2*, 774.

Published on Web 08/05/2010

of the tube and the evidence for "belt" rather than cap nucleation of the nanotube. The core of the paper is the diffraction evidence for the preferred orientation of the single crystal Fe_3C particles on the silica substrate and the clear crystallographic orientation relationship between the particle and the layers of the nanotube. High resolution TEM of the interface between the catalyst particle shows that the surface layers of the carbide which are in contact with the nanotube have reconstructed to form a close packed structure with one of the close packed planes forming the surface. It is this surface which is able to template the graphene layers in an orientation corresponding to each of the two preferred nanotube chiralities which are observed. At each significant stage in the paper, pertinent new references are introduced, and where these are especially numerous they are separately listed and discussed in the Supporting Information.

Experimental Section

Carbon nanotubes were grown by chemical vapor deposition (CVD) in a furnace reactor, at 760 °C under argon, from a solution of 2 wt % ferrocene in 60:40 toluene/1,4-diazine ($C_4H_4N_2$). Dense arrays of nanotubes were grown on fused quartz substrates (with silica purity at the level of 99.99%). The specimens were removed from the silica substrates and dispersed onto holey carbon copper grids for transmission electron microscopy (TEM) analysis. The high-resolution (HR) TEM experiments were performed on a JEOL JEM-4000EX II (400 kV) microscope with a spherical aberration coefficient Cs of 1.07 mm and point resolution of 0.17 nm. No beam damage was observed during TEM studies.

Results and Discussion

Morphology of Nanotubes Grown from Iron Carbide. The direct consequence of the addition of 1,4-diazine ($C_4H_4N_2$) to the hydrocarbon feedstock is that the ferrocene decomposes to deposit catalyst particles of iron carbide (Fe_3C) rather than iron. This behavior is consistent with the role of nitrogen as a carbide stabilizer in steels and cast irons, where it appears to assist the nucleation of the carbide phase via an FeN_x intermediate.[24,25] While there is considerable literature on the nitrogen doping of nanotubes (Supporting Information, part B), the doping issue is not seen as central to this study, and, indeed, our earlier measurements of nitrogen concentrations in the tubes showed that while some nitrogen remains in the core of the nanotubes, both as gas and as adsorbed species, relatively little can be detected in the well ordered walls.[23] In about 50% of the nanotubes in any particular forest, all the concentric layers are either exactly armchair or (not quite so exactly) zigzag, with approximately equal proportions of each type.[22] Some of the internal walls terminate in webs bridging the central core, and interestingly, catalyst particles can be found at both the base and the tip of the nanotube, with evidence that the majority of each nanotube formed from the base particle. Figure 1a is a diagrammatic representation of a typical tube, and Figure 1b shows some TEM micrographs of the catalyst particles at each end and also of the central part of the tube

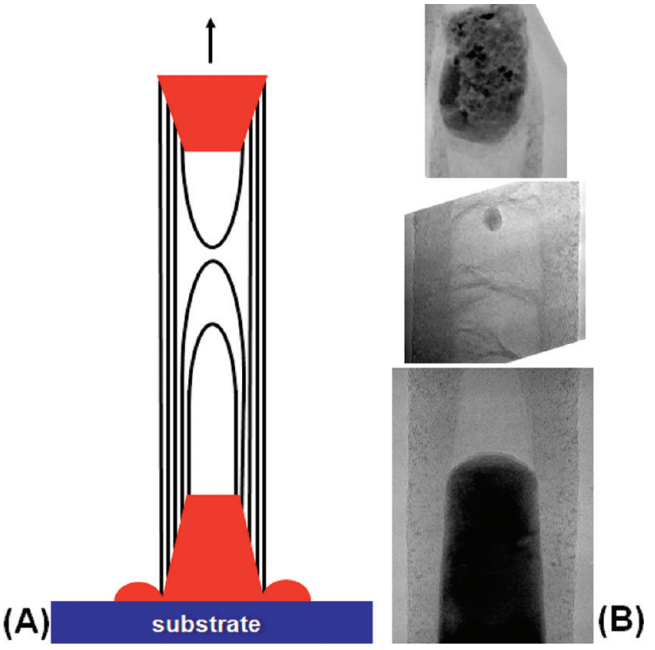

Figure 1. (a) Schematic of a multiwall carbon nanotube grown using heteroaromatic, nitrogen based, compound in the carbon supply. The nanotube has a catalyst particle at both ends with evidence of both base and tip growth, the former accounting for a greater proportion of the nanotube length. The inner layers of the multiwall tube terminate in webs bridging the nanotube bore. (b) TEM micrographs from each end of one nanotube showing the two catalyst particles together with a higher magnification view of the central part of the tube showing the webs bridging the bore. The catalyst particle at the top of the nanotube has oxidized to some degree.

remote from either end. It can be seen that the external walls connect both particles, and the inner walls terminate in webs bridging the central core of the nanotube. The walls toward the center in particular make a small angle with the tube axis which increases as the center hole is approached. The bending of the layers toward the core of the nanotube generates a splay distortion which appears to be density compensated by layers ending abruptly within the structure of a tube. A further significance of such terminations is that they would appear to preclude any scroll mechanism of growth, which in any case would not be consistent with layers terminating in webs. However, one cannot rule out the possibility that the outer layers of the tube, where relatively few terminations occur, are a scroll. A scroll would lead to each layer having the same chirality but not explain why the layers are either armchair or zigzag nor why the chirality is maintained throughout the tube including the layers near to the core.

These somewhat unusual morphological features need to be reconciled with a possible nucleation and growth sequence of the nanotubes. Such a scheme, compatible with the evidence, is shown in Figure 2. The nanotubes nucleate on the sides of the catalyst particle, first encircling the particle as a belt and then, as the belt grows longitudinally, deforming the catalyst particle until it divides, the growth continuing from both ends. Additional layers are then formed internally, and these punch off, cap-wise, from the growing and receding catalyst particles, to give the webs spanning the hollow core of the nanotube. However, the central questions remain as

(24) Jack, K. H. *Proc. R. Soc. London, Ser. A* **1948**, *195*, 41–55.
(25) Uda, M.; Pehlke, R. D. *Trans. Am. Foundry Soc.* **1971**, *79*, 577.

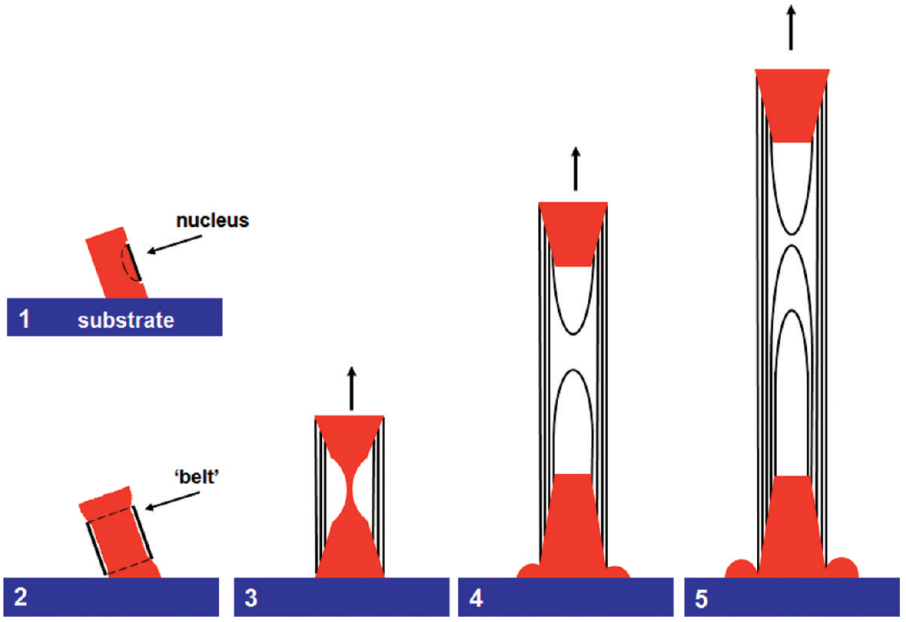

Figure 2. Schematic sequence for growth of nanotubes from iron carbide catalyst. (1) Adsorbed carbon on the surface becomes supersaturated to the point where the excess carbon forms a graphene sheet bound by ledges on the catalyst surface. (2)Layer nucleates both circumferentially and axially until it joins up as a graphene belt encircling the catalyst particle; further layers are added to the embryonic nanotube. (3) The axial growth of the nanotube stretches the mobile catalyst particle until it breaks into two pieces. (4 and 5) The nanotube grows from both ends although more rapidly from the base—probably because of the greater area of carbide exposed to the incoming carbon; the number of layers added to the belt is increased from the inside, and these layers are separately nucleated by "conventional" caps providing the webs which cross the central hole. Note that the crystallographic alignment of the catalyst particles with each other, and indeed with the substrate, will result from the mutual alignment of the growing nanotubes (excluded volume) and would not apply to the first stages of nucleation envisaged in the diagram.

to what determines the chirality of the first graphene layer to be nucleated and, particularly, why this should be the same for each layer of the nanotube.

Diffraction Evidence. The electron diffraction patterns show that the catalyst particles are orthorhombic iron carbide (Fe_3C), and in all cases the central axis of the nanotubes (growth direction) is parallel to $[100]_{carbide}$. Figure 3a shows an electron diffraction pattern from a region which includes both the catalyst particle and the armchair nanotube growing from it. There is a clear crystallographic orientation relationship between the armchair nanotube and the catalyst particle, namely, $\langle 100\rangle_{CNT}$ parallel to $[100]_{carbide}$, with the plane of the graphene layers lying within the [100] zone of the carbide. Figure 3b is a pattern from the same tube but remote from the catalyst particle. In the case of zigzag tubes the orientation relationship is somewhat less perfectly defined where the tube is still in contact with the catalyst particle as shown in Figure 3c, the orientation of the nanotube appearing to be twisted by a few degrees from the exact relationship of $\langle 210\rangle_{CNT}$ parallel to $[100]_{carbide}$. However, the quality of the alignment appears to improve remotely from the catalyst particle, Figure 3d. The 002 reflections (inter-graphene layer spacings) appear as short arcs rather than spots in the diffraction pattern of Figure 3c, confirming the conical angle of some of the nanotube walls (Figure 1a) with respect to the growth axis (max $\pm 7°$ close to a particle, less than $\pm 4°$ in the center of the nanotube).

There is evidence[26] that iron carbide has preferential [100] growth direction, at least when grown with a needle texture in the presence of ferrite in a cast iron, (n.b. these authors label the unit cell differently from the normal convention, so that they describe the growth direction as being along the *b* axis). Our observations are consistent with this report in that we see that $[100]_{carbide}$ is perpendicular to the growth substrate. It should also be noted that approximately 50% of tubes which are neither pure armchair nor pure zigzag would appear to be a mixture of the two types, and such a mixed pattern is shown in Figure S1 (Supporting Information).

While the diffraction patterns tell us that the catalyst crystallographic orientation is closely related to that of the tube axis and that all the catalyst particles growing nanotubes have the same orientation with [100] normal to the substrate surface, they still provide *no* explanation as to *why* the nanotube layers are either armchair or zigzag and not at a more general chiral angle and *why* the structure of each layer is the same in a given nanotube (or part of one).

Evidence for Epitaxy. The literature on the influence of metal catalyst structure on the orientation of graphene layers nucleated on its surface is already considerable. Particular aspects have evolved which focus on the role of crystallographic ledges on the surface of the catalyst crystals, epitaxy with particular (low index) faces, or both. Ding et al.,[27] viewing a chiral nanotube as having a screw dislocation along its axis, performed ab initio

(26) Hartmann, S.; Roppersberg, H. *Mater. Sci. Eng. A* **1995**, *190*, 231–239.

(27) Ding, F.; Larsson, P.; Ahuja, R.; Duan, H.; Rosén, A.; Bolton, K. *Nano Lett*. **2008**, *8*, 463.

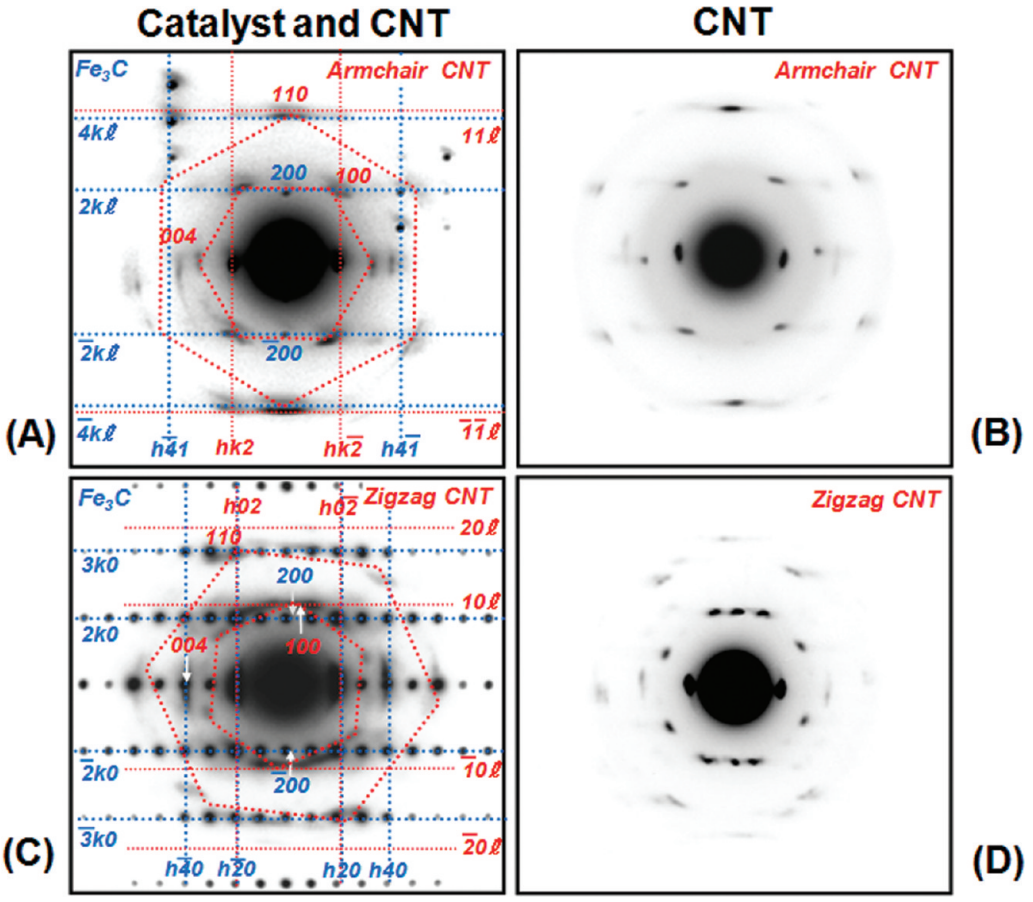

Figure 3. (A) Selected area electron diffraction pattern from a region of an armchair nanotube in contact with the Fe_3C catalyst particle. The blue outlines identify the reciprocal space repeats of the Fe_3C pattern indicating that the tube axis is $[100]_{carbide}$, while the red outlines indicate the salient features of the armchair nanotube diffraction pattern. (B) is a diffraction pattern from an armchair nanotube remote from the catalyst particle. (C) shows the diffraction pattern from another tube where it is in contact with its catalyst particle as well the pattern from the particle, the beam in this case being oriented along $[001]_{carbide}$. Again the tube axis is parallel to $[100]_{carbide}$, but here the tube is zigzag, not armchair. The zigzag structure remote from a particle is shown in (D).

calculations of a graphene layer growing from a ledge on a Ni {111} surface. They suggested that armchair tubes would grow from a suitable ledge with very little energy required to restart "each next carbon ring". Their diagrams (e.g., Figure 2 of ref 27) show that the lattice parameters of close packed cobalt surfaces provided a ready basis for templating graphene surface layers, owing to the close relationship between the close packed metal atom spacings and the C−C distance. Zhu et al.,[28] in a TEM-based study, related the chirality of single wall nanotubes to the angle between the step-edge (ledge) on a Co {111} surface and the eventual growth direction of the nanotube. While this mechanism presented a strategy for chirality control, it is not clear, without any description of the stages between the nucleation of an initial patch on a {111} facet and the emergence of the final nanotube, how the angular relation between the step-edge orientation and the axis of the eventual nanotube would be controlled. Additionally, following a previous report,[29] the authors emphasized the almost perfect fit between the surface interstices of the Co {111} facet and the positions of the carbon atoms in graphene. The same theme of epitaxial control was developed by the modeling work of Reich et al., where they focused on the nucleating patch of graphene as determining the symmetry and structure of the graphene cap and thus the chirality of the resultant nanotube.[30] These authors also point to the significance of local lattice matching between the spacings of Ni atoms (the metal they chose to model) and neighboring carbon atoms. Such local matching is also the basis of a very recent modeling study by Shibuta and Elliott[31] which addressed the organization of carbon atoms on close packed faces of Co and Ni as well as {001} type faces of BCC iron. They demonstrated the organization of different concentrations of carbon on the surface interstices, showing coordinated islands of carbon at low concentrations which gradually joined up as graphitic sheets with increasing concentration toward surface interstice saturation. They also extended this modeling study to include the potential role of close packed facets which form transiently on small, noncrystalline assemblies of atoms, the significance of which stems from an earlier modeling study.[32] The correspondence between the close packed atom spacing in the different metals

(28) Zhu, H.; Suenaga, K.; Wei, J.; Wang, K.; Wu, D. *J. Cryst. Growth* **2008**, *310*, 5473.
(29) Sikka, S. K.; Vohra, Y. K.; Chidambaram, R. *Prog. Mater. Sci.* **1982**, *27*, 245.
(30) Reich, S.; Li, L.; Robertson, J. *Chem. Phys. Lett.* **2006**, *421*, 469–472.
(31) Shibuta, Y.; Elliott, J. A. *Chem. Phys. Lett.* **2009**, *472*, 200–206.
(32) Shibuta, Y.; Muruyama, S. *Chem. Phys. Lett.* **2003**, *382*, 381–386.

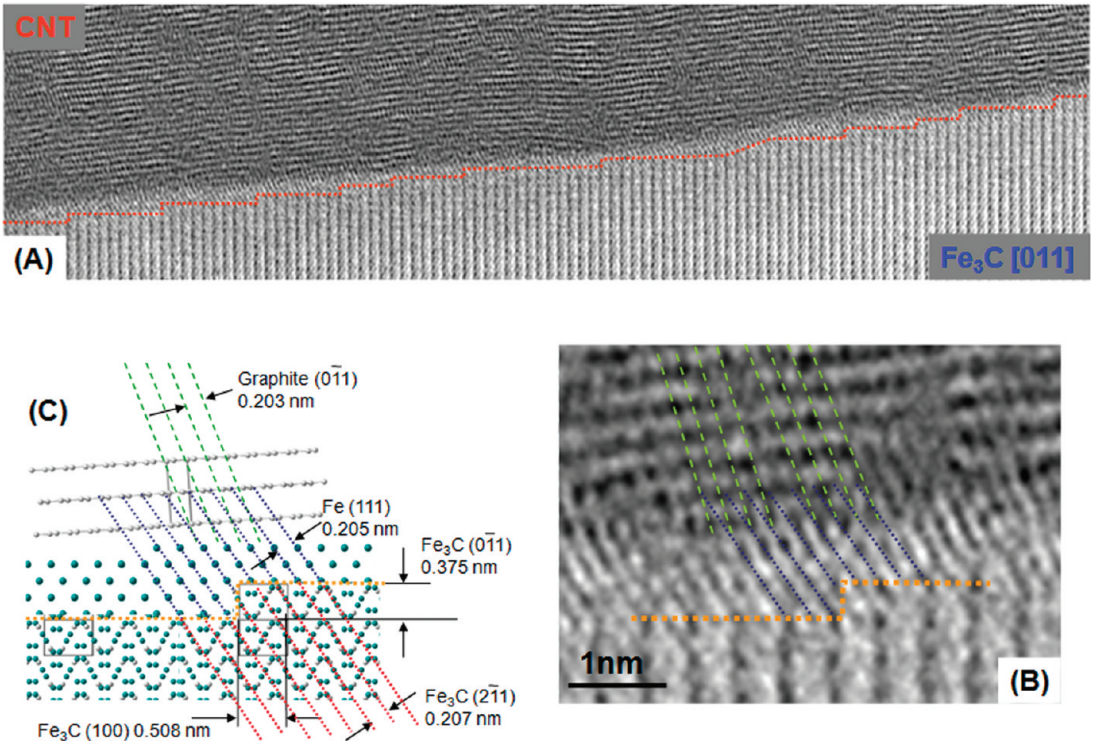

Figure 4. (A) High resolution electron micrograph with the beam axis parallel to $[011]_{carbide}$, giving an edge-on view of an $(0\bar{1}1)_{carbide}$ face of the catalyst particle, which is overlaid by the graphene layers of the nanotube, all of which are zigzag. There is evidence of reconstruction of the carbide structure within a few atomic layers of is surface. The reconstructed region at higher magnification (B) and the ball model representation (C) show planes of spacing the same as the close packed ones in FCC iron at an angle of 70° to the surface layer (dark blue), which is thus compatible with a {111} close packed surface. Interestingly, the imaged oblique planes are at a similar orientation and spacing to the $2\bar{1}1$ planes of Fe_3C (red).

Fe, (0.252 nm), Co, (0.251 nm), and Ni (0.248 nm)) with C−C distance in graphite (0.246 nm) is beguiling and suggests one reason why these three metals are pre-eminent in the growth of nanotubes from metal catalysts. However, the growing indication that this correspondence is a central feature in controlling the orientation of a graphene layer has not yet been translated into a demonstration of chirality control nor into a mechanism which will relate the orientation of the nucleating patch with the tube axis and the chirality of the resulting nanotube. Our multiwall tubes grown from iron carbide, with armchair or zigzag structures only, demonstrate a distinct relationship between catalyst crystal orientation and the structure. However, iron carbide is orthorhombic *Pnma*, $a = 0.51$ nm, $b = 0.67$ nm, and $c = 0.45$ nm, and so is *not* a close packed structure and has no close packed planes.

High-Resolution TEM Evidence. Figure 4a shows a HRTEM micrograph of an edge-on view of the $(0\bar{1}1)$ facet of the orthorhombic crystal (the electron beam direction being $[011]_{carbide}$) and the zigzag nanotube growing from it. Surface steps of 0.375 nm along the $[0\bar{1}1]_{carbide}$ are visible, and graphene layers originate at some of the resultant ledges. Where a given graphene layer runs across the surface of one or more steps, it develops a small angle with respect to the tube axis. The image of the nanotube part shows contrast from both the (002) planes and the (011) planes of graphite (at 72.36°). The presence of the $(011)_{graphite}$ planes is indicative of the *abab* stacking regime possible between successive layers with the same chiral angle. However, we cannot assume that these graphene layers were nucleated from the particular facet seen in edge-view here, as they may have started on another facet of the prism set. Most significantly though, the crystal structure imaged within the Fe_3C lattice is not preserved close to the surface, and only the contrast from $(2\bar{1}1)$ planes is displayed in the image, with 0.207 nm spacing. We interpret the thin surface structure of the carbide as a reconstructed surface layer of iron atoms. The most probable reconstruction will be that which creates a close packed surface. The new planes, where seen clearly, make an angle of $70.5° \pm 1°$ with the surface and are spaced at 0.207 nm, which is close to the 0.205 nm of {111} planes in FCC Fe, implying that the surface can also be interpreted as a close packed (111) plane.

Figure 4b shows a model of this interface region. The reconstruction would appear to preclude carbon at the carbide ratio of 1/3 in the surface layers, although it should be borne in mind that the solubility of carbon in γ Fe at 760 °C is of the order of 3 atom %. However, the concentration of bound carbon on the iron surface will amount (in the limiting geometric case) to two carbon atoms for each surface iron atom. Such surface reconstruction is a known phenomenon[33] and is driven by the energetic advantage of the surface being atomically flat, with the surface metal atoms able to make maximum bonding contact with their neighbors. However, we cannot say from our own evidence whether the reconstruction is favored in any way by the presence of carbon in the surface interstices or whether it is a normal property of

(33) Oura, K.; Lifshits, V. G.; Saranin, A. A.; Zotov, A. V.; Katayama, M. *Surface Science: An Introduction*; Springer-Verlag, Berlin, 2003.

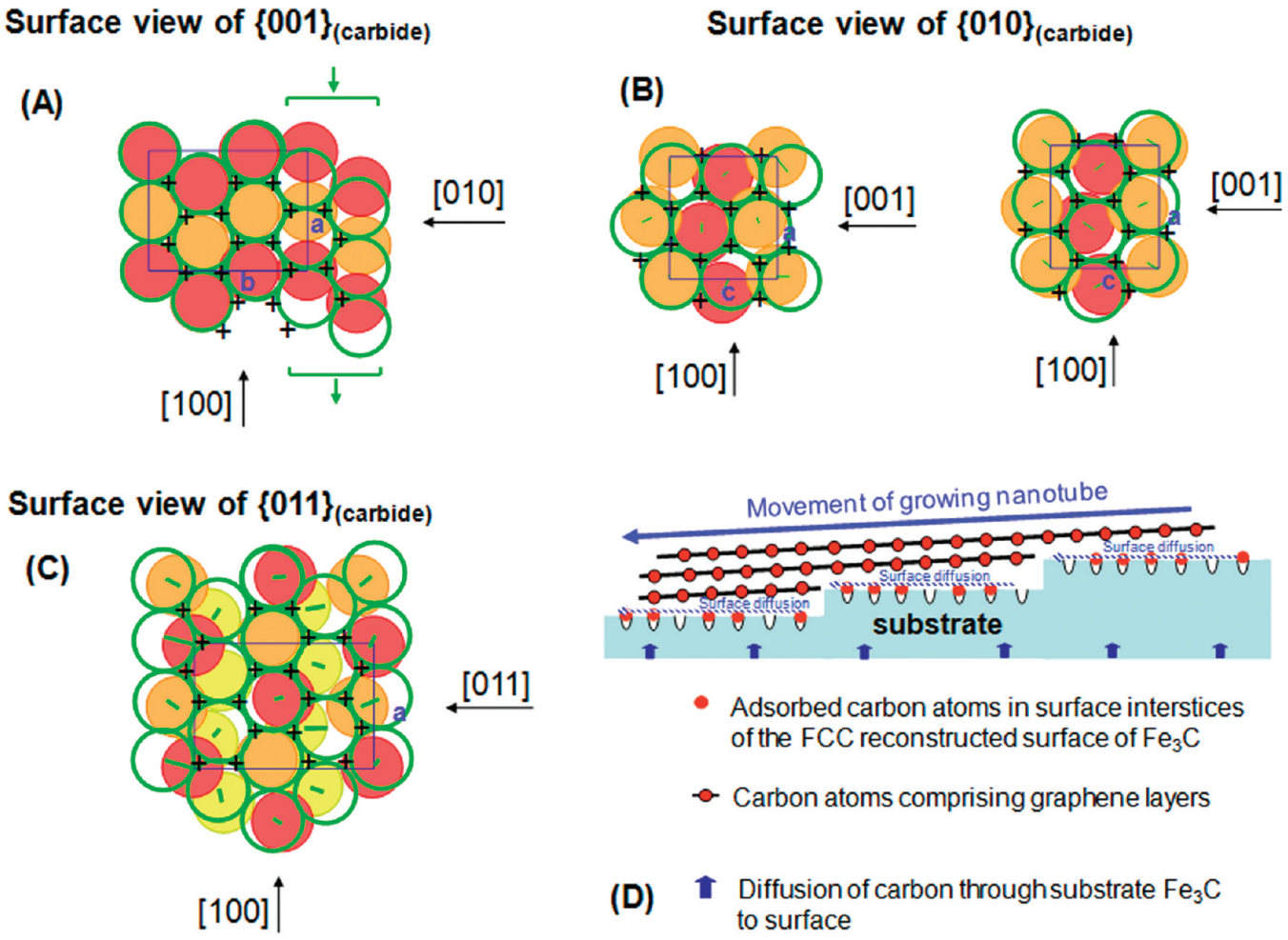

Figure 5. (A, B, and C) Views of the surface of three low index faces of Fe_3C, (001), (010), and (011) which are parallel to the $[100]_{carbide}$ axis and thus to the axis of the nanotube. In each of the diagrams the red atoms are the top layer and the orange atoms the second layer, and in the case of (C), yellow the lowest layer. The projection of the orthorhombic cell is also shown. The green circles show a single reconstructed close packed layer drawn with circle diameters representing the close packed radius of Fe in the FCC structure. The black crosses indicate the hexagonal arrangement of surface interstices in the reconstructed close packed layer. Their spacing is virtually the same as the carbon−carbon atom bonds within the graphene layer, and their role as a template is evident. The crosses have not been connected into a hexagonal net in these diagrams so as to avoid implying that all the carbon bonds are made in the adsorbed layer. The dimensions of the iron carbide orthorhombic unit cell are $a = 0.51$ nm, $b = 0.67$ nm, and $c = 0.47$ nm. (A) is a view of the (001) face of the carbide, showing the top two layers of iron atoms. Bands of the surface along the [100] direction are already very nearly close packed requiring only displacements normal to the surface of $\pm c/8$ to form a close packed layer; these bands are offset from each other (again along [001]), and it is the normalization of this offset, possibly by a dislocation type mechanism which will complete the full reconstruction (as illustrated by the green arrows). The orientation of this close packed reconstructed surface layer would be compatible with an armchair nanotube. (B) View of the (010) face of the carbide, showing two schemes for reconstruction into a single close packed layer. In this example the top two layers are displaced in a direction normal to the face by $b/6$. The first of the reconstruction schemes would produce hexagonal close packed surface layers which would form a template for armchair tubes, the second one for zigzag tubes. In each case the component of atomic displacement in the surface plane is illustrated by the short green lines. (C) View of the (011) face showing the reconstruction which involves movement of the three upper layers of iron atoms in the carbide structure. The movements in the plane of the surface are indicated by the green lines. The movements normal to the surface, to bring the red, orange, and yellow iron atoms into the same surface layer, amount to 1/3 of the carbide unit cell dimension normal to the face. The templating in this case would be compatible with armchair tubes, suggesting that the graphene layers above the (011) face seen in Figure 4 may not have nucleated on that face and take their orientation from the face where they nucleated. (D) A schematic view of the generation of carbon nanotube layers of the same chirality via surface templating from the reconstructed surface faces of the catalyst particle. In reality there is no evidence that each surface step of the catalyst corresponds to a graphene layer, and a mismatch between the spacing of the active steps and the graphene layers appears to be accommodated by the graphene layers not lying exactly parallel to the [100] axis of the catalyst.

such an Fe_3C facet at 760 °C. It is useful to note that surface melting of Fe_3C has been proposed on the basis of molecular dynamics simulations at a temperature below 923 °C,[34] so it is not difficult to accept that there will be sufficient atomic mobility to permit surface reconstruction at a growth temperature of 760 °C. Figure S2 (Supporting Information) shows a high resolution micrograph similar to that of Figure 4, except in this case the orientation is different with the facet seen edge-on being $(001)_{carbide}$. Figure S3 (Supporting Information) shows an edge-on of the $(001)_{carbide}$ facet with a surface step associated with the termination of a graphene layer.

The structure and orientation of the catalyst−nanotube interface are difficult to study, and other techniques like electron energy loss spectroscopy or energy dispersive X-ray spectroscopy are not likely to provide more detailed analysis of this interface.

Surface Reconstruction. Structural implications of the surface reconstruction of Fe_3C, on the low-index prism faces

(34) Ding, F.; Bolton, K.; Rosen, A. *J. Vac. Sci. Technol. A* **2004**, *22*, 1471–1476.

such as (010), (001), and (011), determine the minimum rearrangement routes which will convert the surface of the Fe_3C crystal into {111} faces. Figure 5 shows the minimum rearrangement routes for the surface for the (001), (010), and (011) faces, respectively, between the Fe_3C structure, and surface close packed planes are now addressed. It can be seen (Figure 5a) that the (001) surface already contains hexagons of the close packed structure which would be compatible with armchair tubes, while small shears along the *a* axis coupled with modest movements in the *c* axis direction ($\pm c/8$) normal to the surface as the top two layers merge into one. For the 010 surface, the most direct rearrangement to a close packed surface would appear to be that shown in Figure 5b (top), within this case movements normal to the surface amounting to $\pm b/12$. Here the hexagonal surface structure arising is rotated by 30° with respect to the *a* axis (nanotube growth axis) compared with the reconstructured surface of 001 and would thus be compatible with the formation of zigzag nanotubes. Figure 5b (lower) shows an alternative scheme for the reconstruction of the 010 face, which involves slightly greater movements, but produces an orientation of the surface hexagons the same as for the reconstructed 001 face and thus compatible with armchairs. Figure 5c shows the possible scheme for the 011 faces, indicating in this case an armchair nanotube. The atomic movement required for these reconstructions is really very modest. One can understand why this should be for the (010) and (001) faces by comparing the area of a close packed layer of iron atoms, referenced to the nonprimitive rectangular cell, of 1.13 nm^2 with that for the *ab* face of $Fe_3C_{orthorhombic}$ of 3.44 nm^2 and that for the *ac* face of 2.30 nm^2. The ratio of these areas is very close to a simple 1:3:2, showing that the areal packing density of the top two layers of iron for each face is very close to that in a single close packed layer of Fe atoms. There is no such simple ratio for (011) as the reconstruction involves the top three layers of iron atoms in the carbide.

Each of the reconstruction schemes which give close packed surfaces of iron atoms has surface hexagons in an orientation which preserves the mirror symmetry of the Fe_3C catalyst. Put another way, the symmetry of the underlying "mother" crystal prints through to control the orientation of the reconstructed hexagonal surface about its normal, limiting it to orientations compatible with armchair and zigzag only.

Why Does Close Packed FCC Iron Not Template Nanotubes of Fixed Chiral Angles? If the critical surface layers of Fe_3C reconstruct to FCC (Fe), what is special about Fe_3C as a catalyst? It should be noted that the growth of multiwall carbon nanotubes from a single crystal of γ-Fe cannot benefit from the hexagonally structured faces as these are tetrahedrally disposed with respect to each other and thus not compatible with the uniaxial symmetry of a nanotube. Furthermore, there is no evidence that the iron catalyst particles show any special crystallographic relationship with the substrate, whereas the Fe_3C crystals appear to grow along the [100] direction in agreement with earlier reports.[26] Interestingly, a report of nanotube growth from nickel particles magnetically oriented with ⟨111⟩ normal to the substrate[35] makes no suggestion of chirality control of the nanotubes, so the crystallographic orientation of the catalyst particles, while possibly a necessary condition, is not apparently a sufficient condition for the growth of tubes with a uniform chiral angle.

Discussion of Model of Catalyst Control of Chiral Angle. We now need to address the fundamental issues: if the iron carbide catalyst is mobile at the temperature of synthesis, as indeed it may be, having molded to the internal form of the nanotube, then why should the crystal orientation of the carbide be stable, as evidenced by the fact that catalyst particles are preferentially oriented, with $[010]_{carbide}$ parallel to the nanotube axes and indeed to either [100] or $[210]_{graphene}$, and why is the constant chirality maintained along the entire length of the tube? In the in situ TEM study of Yoshida et al.[36] of a multiwall nanotube growing from a 10 nm carbide particle in much more dilute gaseous environments than we used and also not in the presence of nitrogen, there is apparently no predisposition to a particular chirality, and the orientation of the carbide is observed to vary on a time scale of ~1 s. Our carbide particles are ~1000× the volume of those used in the in situ experiments, where there is also the possibility that the atomic mobility is also enhanced by beam momentum transfer resulting in an increased vacancy concentration, as well as by disruptive influences from electrostatic interaction with the beam. Both factors suggest that less mobility would be experienced in our experiments. Nevertheless, we cannot rule out the possibility of some mobility over the time scale of our experiment. However, we point out that epitaxy is a two way street. If the surface orientation of the carbide is compatible with the orientation of the nanotube at the point of nucleation of the tube, then the fact that the growing nanotubes are forced to align parallel to each other as they grow because of excluded volume constraints means that the epitaxy will help to maintain crystallographic orientation of the carbide crystals against any disruptive force such as carbon diffusion (suggested in ref 36). Rather than seeing the possibility of mobility as a challenge to our evidence for epitaxy, we see the fact that the orientation of all the carbide particles is nearly the same, despite their potential internal mobilities, as providing additional evidence for epitaxy enabling the alignment of the nanotubes to preserve the alignment of the particles. Indeed, we relate this observation directly to the prediction of Yoshida et al., that epitaxial control of catalyst orientation would "have further implications for chirality control". We suggest, however, that this control is derived from the mutually aligned nanotubes and not from the substrate as envisaged in ref 36.

(35) Fowlkes, J. D.; Melechko, A. V.; Klein, K. L.; Rack, P. D.; Smith, D. A.; Hensley, D. K.; Doktycz, M. J.; Simpson, M. L. *Carbon* **2006**, *44*, 1503–1510.

(36) Yoshida, H.; Takeda, S.; Uchiyama, T.; Kohno, H.; Homma, Y. *Nano Lett*. **2008**, *8*, 2082–2086.

It appears that in our system we have achieved the preferential growth of the carbide in the $[100]_{carbide}$ direction normal to the quartz substrate and that this is one key factor in the growth of the tubes with only one of two chiral angles (equivalent to armchair or zigzag). The second key is our observation of the role played by the reconstructed surface layers of the low index faces of the [100] zone of the carbide crystals to provide close packed iron surfaces capable of templating graphene layers. It appears that the orientation of the reconstructed surface hexagons of iron about their normals takes on the mirror symmetry of the orthorhombic Fe_3C particles meaning that the graphene nuclei will also have that symmetry and thus grow into either armchair or zigzag tubes. Competing nucleation events may also occur on the facets of the $[100]_{carbide}$ zone meaning that they also create graphene layers parallel to the zone and thus to the tube axis, with the only proviso that more than one nucleation site may lead to mixed armchair and zigzag tubes, as indeed are seen. While a close packed facet on a γ iron particle may well generate graphene layers of a particular orientation, there is no underlying crystallographic relationship (as there is with orthorhombic iron carbide) which would determine the relationship between the growing graphene nucleus and the eventual tube axis.

In the cap nucleation model the catalyst particles often show fluctuations in their structure and orientation.[30] Furthermore, the energy difference between formation of caps leading to a particular chirality of nanotubes is so small that there is no reason one cap should be preferred over another,[37] and hence strategies for chirality control in this model may be difficult to achieve. In our model of belt nucleation the orientation of the catalyst particles is present because of the preferential growth during nucleation. Furthermore, these well-defined particles have the capability of surface reconstruction to form close packed surface layers capable of templating graphene layers of primitive structures with zigzag and armchair orientation and with a spatial symmetry which is uniaxial and thus compatible with the nanotube.

The result of this study, while explaining the observation of multiwall nanotubes in which all the layers have a single chiral angle of either 0° or 30°, points to future strategies involving low symmetry catalyst particles which have the capability of surface reconstruction to form close packed surface layers capable of templating graphene layers of predetermined orientation. Such strategies may involve the growth of large iron (or cobalt or nickel) carbide crystals to explore the possibility of their crystallographic surfaces being used for growth of single graphene sheets, as well as the creation and maintenance of truly nanoscale particles to achieve growth of single wall tubes of either zigzag or armchair orientation. Strategies to predetermine whether such tubes would be all armchair or all zigzag are not as obvious, but it is possible that the catalyst particles can be grown with impurities which may favor one pair of faces of the [100] zone over others.

Acknowledgment. The authors thank Professor Milo Shaffer, Professor Paul Midgley, and Sebastian Pattinson for stimulating discussions. The authors are also grateful to a referee for pointing out the potential relevance of carbide catalyst mobility to the experiments reported here. K.K.K.K. and C.D. thank The Royal Society for funding.

Supporting Information Available: Further references and commentary and additional figures (PDF). This material is available free of charge via the Internet at http://pubs.acs.org.

(37) Zhu, W.; Börjesson, A.; Bolton, K. *Carbon* **2010**, *48*, 470.